Earth and Planetary Science Letters 441 (2016) 178–187

Contents lists available at ScienceDirect

Earth and Planetary Science Letters

www.elsevier.com/locate/epsl

Geological evolution of the marine selenium cycle: Insights from the bulk shale $\delta^{82/76}$Se record and isotope mass balance modeling

Kristen Mitchell [a], Sannan Z. Mansoor [a], Paul R.D. Mason [b,*], Thomas M. Johnson [c], Philippe Van Cappellen [a]

[a] Ecohydrology Research Group, Department of Earth and Environmental Sciences and Water Institute, University of Waterloo, Waterloo, Canada
[b] Department of Earth Sciences, Utrecht University, Budapestlaan 4, 3584 CD Utrecht, The Netherlands
[c] Geology Department, MC-102, University of Illinois, Urbana-Champaign, Urbana, IL 61801, USA

ARTICLE INFO

Article history:
Received 26 March 2015
Received in revised form 11 February 2016
Accepted 13 February 2016
Editor: M. Frank

Keywords:
selenium
stable isotopes
marine biogeochemical cycling
isotopic mass balance modeling
geological evolution

ABSTRACT

Bulk $\delta^{82/76}$Se values of representative marine shales from the Paleoarchean to the present day vary between approximately −3 and +3‰ with only local deviations beyond this range. This muted Se isotope variability in the shale record contrasts with the relatively large fractionations associated with abiotic and microbial Se oxyanion reduction seen in experimental studies. Long-term temporal trends in the bulk shale data do not directly correlate with changes in redox conditions of the global ocean, although a minor but significant shift towards more negative formation-averaged $\delta^{82/76}$Se values appears to track oxygenation of the deep ocean at the end of the Proterozoic. We hypothesize that extensive $\delta^{82/76}$Se variability in the shale data was suppressed due to the early emergence of biological assimilatory uptake and the resulting persistence of low seawater Se concentrations, coupled with small authigenic Se outputs throughout most of geological time. In the modern ocean, Se is an essential micronutrient with a relatively short residence time of about 11,500 yrs. The marine Se cycle is dominated by assimilation into biomass and subsequent recycling in the water column and surface sediments, i.e. processes that result in only minimal isotopic fractionation. We suggest that similar processes dominated back through the geological record to Archean times. Our model shows that paleoceanographic information could in principle be extracted from proxy data on the Se isotopic composition of seawater, once isotopic differences can be readily discerned between individual sedimentary Se pools.

1. Introduction

Selenium (Se) is an essential micronutrient whose cycling in the modern ocean is primarily controlled by uptake by phytoplankton and subsequent recycling to the water column (Harrison et al., 1988; Price, et al., 1987; Wrench, 1978). Selenium occurs in the oceans in different oxidation states, including Se(IV), Se(VI), Se(0) and Se(-II). Most of the dissolved forms of Se are bioavailable and can be assimilated into cells where Se is used, among other functions, to produce selenocysteine, an amino acid found in all three domains of life (Copeland, 2005).

With multiple oxidation states and six stable isotopes, Se-based proxies have the potential to yield important paleoenvironmental information (e.g., Stüeken et al., 2015a; Pogge Von Strandmann et al., 2015). In particular, $\delta^{82/76}$Se values preserved in marine shales are expected to depend on the isotopic compositions of the Se inputs from continental weathering and volcanic plus hydrothermal activity, as well as oceanic processes that fractionate Se isotopes. With respect to the latter, laboratory experiments have shown that microbial and low temperature abiotic reduction of Se oxyanions can impart relatively large fractionations (up to 13.7‰; Ellis et al., 2003; Herbel et al., 2000, 2002; Johnson and Bullen, 2004, 2003). Large equilibrium fractionations of up to 30‰ calculated by Li and Liu (2011) hint at the potential for even greater shifts. Thus, changes in oceanic redox conditions might be expected to influence bulk shale $\delta^{82/76}$Se values.

In a recent study, Stüeken et al. (2015b) compiled all previously published bulk Se isotope compositions of marine sediments and sedimentary rocks (Johnson and Bullen, 2004; Shore, 2010; Mitchell et al., 2012), and added 202 new analyses to generate a detailed record extending back to 3.2 Ga. Currently available data are derived exclusively from bulk shales; Se isotope measurements of various sediment fractions remain under development and only exist for a single Permian marine shale sample (Stüeken et al., 2015c). The vast majority of the bulk shale $\delta^{82/76}$Se values ranged

* Corresponding author.
E-mail address: p.mason@uu.nl (P.R.D. Mason).

http://dx.doi.org/10.1016/j.epsl.2016.02.030

from −1.5‰ to +2.2‰. This variability is equivalent to 2.6 times the standard deviation (1σ) around the mean value of 0.36‰ for the whole data set, a rather small range given the known potential for isotopic fractionation during Se oxyanion reduction (Ellis et al., 2003; Herbel et al., 2000, 2002; Johnson and Bullen, 2004, 2003). The lack of strong isotopic contrast in fine-grained, bulk shale samples has been attributed to the fact that authigenic, reduction-derived Se is not the dominant form of Se incorporated into these rocks (Mitchell et al., 2012; Stüeken et al., 2015b). Se is a micronutrient present only at trace levels in the marine environment (Cutter and Bruland, 1984). Accordingly, organically bound Se, which is weakly fractionated relative to seawater (Mitchell et al., 2012), appears to be the dominant form of Se in organic-rich mudrocks (Kulp and Pratt, 2004). This diminishes the impact of the more highly fractionated authigenic Se. Despite this muting effect, a systematic, statistically significant shift in $\delta^{82/76}$Se from weakly positive Precambrian values ($+0.42 \pm 0.45$‰) to weakly negative Phanerozoic values (-0.19 ± 0.59‰) has been identified and attributed to increased deep-ocean Se oxyanions in the oxic Phanerozoic oceans (Stüeken et al., 2015b). Here, we present 54 new bulk Se isotopic compositions measured on Archean and Proterozoic marine shales and review the rapidly growing database of $\delta^{82/76}$Se for geological materials. The combined results reinforce the conclusions of Stüeken et al. (2015b), showing relatively small amounts of Se isotope fractionation extending back to 3.25 Ga, and with a minor but significant change to lower values in the late Proterozoic.

The developing understanding of the sedimentary Se isotopic record shows that Se isotopes have unique properties as a paleoenvironment proxy. Notably, the marine isotopic Se record differs greatly from the sulfur record. Variations in δ^{34}S of sedimentary pyrite have yielded a wealth of insights into many facets of Earth's evolution, including the emergence of microbial pathways, the oxygenation of oceans and atmosphere, and the abundance of seawater sulfate (Berner and Canfield, 1989; Canfield, 2004; Canfield et al., 2000, 2007; Canfield and Raiswell, 1999; Canfield and Teske, 1996). Selenium and sulfur are both redox-active chalcogens with multiple stable isotopes. They are biochemically essential elements and are involved in metabolisms that likely evolved early during Earth history (Bontognali et al., 2012; Brocks et al., 2003; Eigen et al., 1989; Sun and Caetano-Anollés, 2009). However, these elements have strongly contrasting biogeochemical cycles, since sulfate is a major seawater constituent that exhibits near-conservative behavior and a long oceanic residence time, while Se is a rapidly-cycled trace nutrient (Canfield et al., 2005; Cutter and Bruland, 1984). In this paper, we highlight differences between the marine sulfur and selenium isotope systematics, to illustrate the unique properties of the Se isotope proxy. We also use the S isotope record to highlight the major changes in the redox state of the Earth's surface environment that are not seen in bulk rock Se isotope data.

Recent studies have presented conceptual models that provide a framework for interpreting Se isotope variations in sedimentary rocks (Mitchell et al., 2012; Wen et al., 2014; Stüeken et al., 2015b). These models illustrate qualitatively how sedimentary Se isotope fluxes respond to changes in the global and/or local Se cycle. To evaluate the sensitivity of bulk shale Se isotopic signatures to changes in paleoceanographic conditions and processes, we present a quantitative isotope mass balance model for the marine Se cycle. Our model incorporates all the currently available information on the modern oceanic Se budget and Se isotopic systematics. Next, we simulate how the model responds to relatively large perturbations of the processes controlling the distribution of Se among various pools within the water column and sediments. The model results illustrate the causes of the observed limited variability of bulk shale Se isotopic compositions. More importantly, the results provide quantitative predictions for the variation to be found in the authigenic and organically bound Se fractions' Se isotope compositions, once analytical methods are fully developed to measure them.

2. Marine bulk shale Se isotopes through time

Published marine shale Se isotopic compositions for the Phanerozoic and Archean (Mitchell et al., 2012; Shore, 2010; Stüeken et al., 2015a, 2015b; Wen et al., 2014) are supplemented here with 54 new bulk $\delta^{82/76}$Se values measured on ~30 Archean and Proterozoic shale samples. We selected exceptionally fresh material, mostly collected from drill-cores, for which ancillary trace element and stable isotope data as well as geochronological information are available. The samples cover a broad set of ages and depositional environments, with whole-ocean or basin conditions ranging from anoxic, via euxinic and ferruginous, to fully oxic. The samples were donated by a diverse group of researchers who are identified in the Supplemental Information, together with the sample identity and the host geological formation (Table EA 1). The bulk Se concentrations and $\delta^{82/76}$Se values determined on the individual samples are listed in Table EA 1, and $\delta^{82/76}$Se values are plotted in Fig. 1A. Sulfur isotope compositions over the same time interval are shown, in Fig. 1B, to give a comparative framework of changes in ocean conditions.

The sample preparation and Se isotopic analyses summarized in the Supplemental Information are identical to those described in detail by Mitchell et al. (2012). Estimated uncertainty is ±0.16‰ (95% confidence). To detect any long-term trends in the $\delta^{82/76}$Se data, we grouped the samples into three time intervals: (1) Phanerozoic; (2) Precambrian after the Great Oxidation Event (GOE) and (3) Precambrian before the GOE. The GOE marks the transition to an oxygen-containing atmosphere, whilst the onset of oxygenation of the oceans occurred towards the end of the Proterozoic. Both transitions thus offer key time markers to assess the effect of global changes in earth surface redox conditions on the marine shale Se isotope record. The mean and median $\delta^{82/76}$Se values, as well as their variability, are shown in Fig. 2A. Sulfur isotope variability is shown for comparison and as a reference scale for changing redox conditions in Fig. 2B.

Average seawater Se concentrations in the modern ocean are <1 nM (Cutter and Bruland, 1984), while total Se concentrations in marine sedimentary rocks generally do not exceed a few ppm. The low abundance of Se has so far prevented the systematic isotopic characterization of individual sedimentary phases, for example elemental Se, organic Se and sulfide Se. Thus, at present, the dataset only includes bulk shale $\delta^{82/76}$Se values. The interpretation of the sedimentary $\delta^{82/76}$Se record is further hindered by the absence of independent determinations of the isotopic Se composition of seawater through time, because of the very low Se concentrations in mineral phases that can capture this component such as evaporites (Nriagu, 1989b). Even for modern seawater, direct measurements of the Se stable isotopic composition are currently lacking, and due to Anthropogenic influences would be altered from the natural variations over time. With these limitations in mind, we can provide only a first-order assessment of the marine $\delta^{82/76}$Se record through time.

The bulk shale $\delta^{82/76}$Se values from 3.25 Ga to present generally vary between −3 and +3‰ (Fig. 2A). One strongly positive value 3.04 ± 0.21‰ is from Stüeken et al. (2015b), this sample also has a relatively high Se concentration of nearly 30 ppm. Stüeken et al. (2015a) for instance suggest that the positive $\delta^{82/76}$Se excursions of up to 2.1‰ in the 2.5 Ga Mount McRae Shale formation may have recorded an episode of O_2 production prior to the GOE. Wen et al. (2014) observe a $\delta^{82/76}$Se minimum outside this range of -5.09 ± 0.24‰ with a high selenium content of 121 ppm. This is

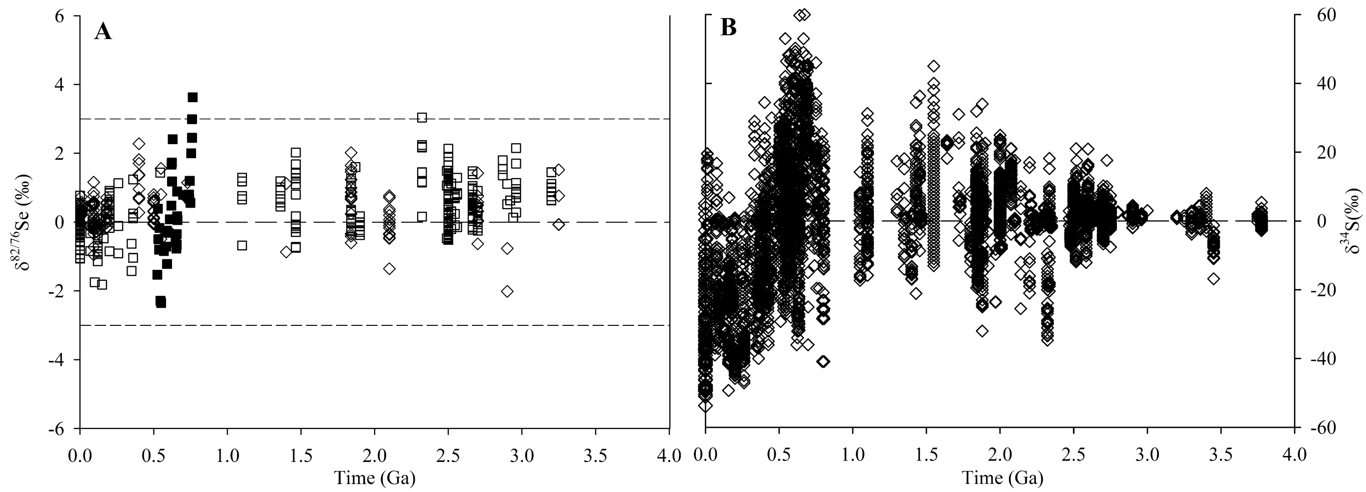

Fig. 1. A) Selenium isotopes through time; samples shown on the figure include 54 new samples from this study plus samples from Mitchell et al. (2012) shown in open diamonds. Data from Stüeken et al. (2015a, 2015b) and Shore (2010) are shown as open squares and data from Pogge Von Strandmann et al. (2015) are shown as closed squares. B) Sulfur isotopes through geologic time, replotted after Canfield and Raiswell (1999). Note the different y-axis scales for $\delta^{82/76}$Se and δ^{34}S.

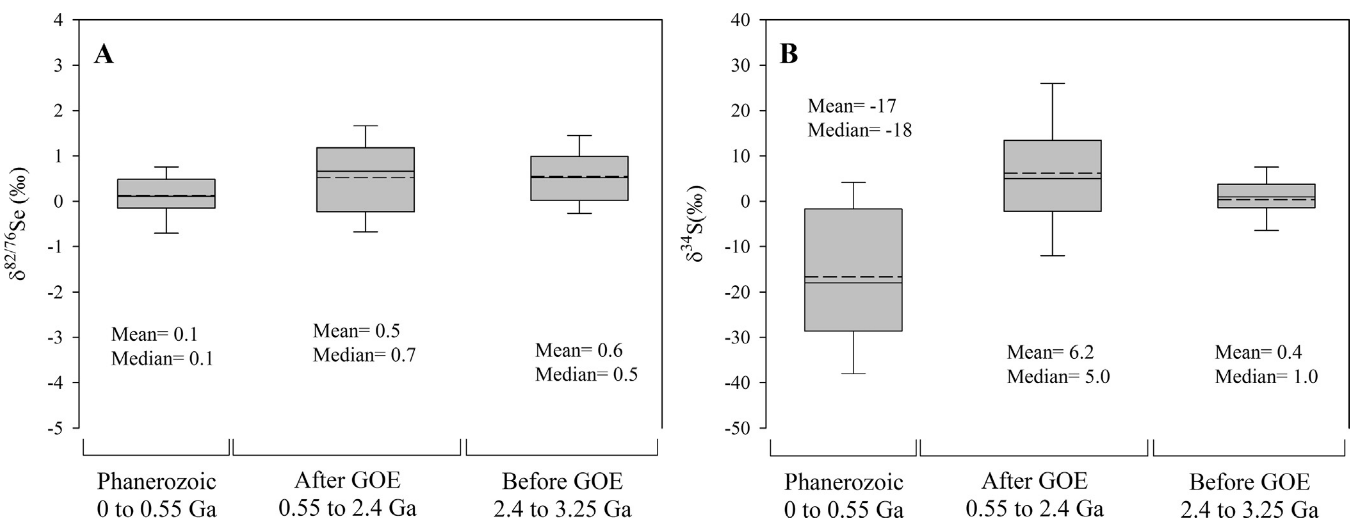

Fig. 2. Box and whisker plots summarizing Se and S isotope data, the 'whiskers' represent the maximum and minimum values in the given ranges excluding the outliers. A) Bulk $\delta^{82/76}$Se of marine sedimentary rocks are divided into three time periods: 1) Precambrian before the Great Oxidation Event (GOE), 2) Precambrian after the GOE, and 3) Phanerozoic. Samples included in the figure includes 54 new samples from this study plus samples from Mitchell et al. (2012). Data from Stüeken et al. (2015a, 2015b), Shore (2010) and Pogge Von Strandmann et al. (2015) are also included. B) δ^{34}S of sulfides from nearly 5000 samples (Canfield and Farquhar, 2009) separated into the same 3 time intervals: 1) 1096 samples, 2) 2531 samples, 3) 945 samples. The solid line within each box represents the median and the dashed line the mean. Note the different y-axis scales for $\delta^{82/76}$Se and δ^{34}S.

a large amount of Se compared with values reported in this study and Mitchell et al. (2012) whose samples rarely surpass 10 ppm and do not exceed 100 ppm Se. Stüeken et al. (2015a, 2015b) report only one value above 100 ppm and few exceed 10 ppm Se. The data reported by Wen et al. (2014) are not included in our compilation, because these appear to reflect the special case of local ferruginous conditions in an otherwise oxic ocean (see discussion below), rather than a global shift. Some of the extreme values in the Pogge Von Strandmann et al. (2015) data set may reflect similar regimes.

The mean and median $\delta^{82/76}$Se values are close to 0‰, but slightly positive prior to the Phanerozoic. No detectable change occurs across the GOE. A decrease of less than 0.5‰ is seen from the Precambrian to the Phanerozoic mean values, possibly reflecting a slight secular change in the isotopic Se composition of seawater. These observations from our new data compilation confirm similar interpretations previously made by Stüeken et al. (2015b). The minor differences in shale $\delta^{82/76}$Se values across the GOE and Precambrian–Phanerozoic transitions contrast strongly with the large shifts in the sulfide δ^{34}S record (Fig. 1 and Fig. 2). Sulfide δ^{34}S values are not directly comparable to bulk rock $\delta^{82/76}$Se, but they illustrate some of the changes in redox conditions that might have been expected to influence the Se isotope record. Pyrite δ^{34}S reflects increases in seawater sulfate concentration and the importance of microbial sulfate reduction following the GOE (Berner and Canfield, 1989; Canfield et al., 2000; Canfield, 2005; Canfield and Farquhar, 2009) (Fig. 1B). The abundance of Se oxyanions in the ocean through time remains unknown, but might have been expected to show similar increases during progressive oxygenation of the Earth's surface environment (Stüeken et al., 2015b). The Phanerozoic S isotope record is characterized by the occurrence of very negative sulfide δ^{34}S values that reflects the reduction in sulfide burial and transport into the mantle through subduction in an oxic ocean (Canfield, 2004). Similar processes may have affected the shale $\delta^{82/76}$Se record (Stüeken et al., 2015b).

Although isotopic fractionations have been shown for a variety of processes in the sulfur cycle, including disproportionation reactions (Böttcher and Thamdrup, 2001), microbial sulfate reduction is likely the primary cause of the large S fractionations observed in the sedimentary pyrite record (Canfield et al., 2000; Chambers, 1975; Ellis et al., 2003; Habicht and Canfield, 1997; Harrison and Thode, 1958; Kaplan and Rittenberg, 1964; Krouse and Thode, 1962; Sim et al., 2011; Thode et al., 1951; Wortmann et al., 2001). The range in sulfide δ^{34}S values observed over geological time exceeds the maximum fractionations typically measured in experimental studies of microbial sulfate reduction. In contrast, the opposite is observed with bulk rock $\delta^{82/76}$Se data where the fractionations observed in microbial Se reduction experiments (Ellis et al., 2002; Herbel et al., 2000) greatly exceed the −1.5‰ to +2.2‰ range seen in the vast majority of samples of the shale $\delta^{82/76}$Se record.

Large variations in $\delta^{82/76}$Se values have been observed in some highly-enriched Se deposits associated with black shales. These variations, however, have been attributed to Se enrichment and isotopic fractionation accompanying post-depositional hydrothermal or weathering-related alteration processes (Wen and Carignan, 2011; Wen et al., 2007; Zhu et al., 2008, 2014). Hence, we attribute the very different features observed in the marine bulk shale $\delta^{82/76}$Se and sulfide δ^{34}S records to the fundamentally different oceanic cycling of Se, relative to S.

The fate of Se in today's ocean is dominated by assimilatory uptake of aqueous Se oxyanions, and likely other dissolved and colloidal Se forms, followed by efficient re-mineralization of organically-bound Se (Cutter and Bruland, 1984; Suzuki et al., 1979). As a result, vertical distributions of dissolved Se in the modern ocean are nutrient-like, with extremely low concentrations in the photic zone (Cutter and Bruland, 1984; Cutter and Cutter, 1995; Measures and Burton, 1980; Measures et al., 1983). The degree to which the same nutrient behavior of Se applies to earlier geological times has not been well constrained. However, we hypothesize that the muted long-term trend of the average shale $\delta^{82/76}$Se values, plus the relatively small range observed for the entire data set (Fig. 1A and Fig. 2A), is best explained by a limiting availability of Se in marine surface waters persisting throughout most of the geological record since 3.25 Ga.

To help better understand marine Se isotope dynamics, the next section presents an isotope mass balance model based on currently existing information on the speciation and isotopic composition of Se inputs to the modern ocean. The model calculates the steady state isotopic ratios of the various reactive Se reservoirs in the modern ocean, using representative fractionation factors. Next, the system is perturbed to determine the sensitivity of the Se isotopic ratios of seawater and marine shale to large changes in whole-ocean conditions and marine Se cycling.

3. Selenium isotope mass balance model

3.1. Marine Se cycle: reservoirs and fluxes

The modern, pre-anthropogenic marine biogeochemical Se cycle summarized in Fig. 3, Table 1 and Table 2 is based largely on the work of Suzuki et al. (1979), Nriagu (1989a) and Cutter and Bruland (1984). The biogeochemical Se reservoirs considered in the model are elemental Se(0) which we consider to be in colloidal form (i.e. insoluble), dissolved inorganic Se (DISe), dissolved organic Se (DOSe) and particulate organic Se (POSe). Given the paucity of data on the isotopic fractionations associated with the assimilatory uptake of selenate ($SeO_4{}^{2-}$) and Se(IV) ($HSeO_3{}^{-}$ + $SeO_3{}^{2-}$) (Johnson and Bullen, 2004), and also given the similar range of isotope fractionations associated with the dissimilatory reduction of $SeO_4{}^{2-}$ and Se(IV) (Herbel et al., 2000), the two inorganic species are grouped together as DISe. The organic Se pools are assumed to be composed mainly of selenocysteine, selenomethionine and other reduced Se compounds. Volatile organic forms of Se in the atmosphere are represented collectively as dimethyl selenide (DMSe) (Amouroux et al., 2001). In addition to Se(0) and POSe, Se may be buried in marine sediments as reduced, iron-bound Se (FeSe), as described below. The Se cycle is assumed to be at steady state.

Estimates of Se reservoir masses are given in Table 1. Briefly, the masses of atmospheric Se, total dissolved Se in surface and deep waters, surface ocean POSe, and total sedimentary Se are the same as in the budget of Nriagu (1989a). The total dissolved Se masses are partitioned between DISe and DOSe based on the concentration data of Cutter and Bruland (1984). The (very small) mass of surface water Se(0) is an estimate extrapolated from the very limited data reported for nearshore environments (Doblin et al., 2006; Takayanagi and Wong, 1983). The mass of POSe in the deep waters is calculated from representative values for the concentrations of total particulate matter and particulate Se (Buat-Menard and Chesselet, 1979; Mackenzie et al., 1979). The total sedimentary mass of Se is divided into three reservoirs (Se(0), POSe and FeSe) based on average relative abundances derived from data for marine sediments and shales (Cutter, 1985; Fan et al., 2011; Kulp and Pratt, 2004; Mitchell et al., 2012; Sokolova and Pilipchuck, 1973; Velinsky and Cutter, 1990; Wen and Carignan, 2011; Wen et al., 2007; Wen and Qiu, 1999).

Fluxes that are well documented in the literature are imposed directly into the model; others are estimated by considering the underlying process(es). For example, the diffusive fluxes of DISe and DOSe between surface and deep ocean layers are computed by multiplying the concentration gradients between the midpoints of the surface water and deep water layers with a representative vertical eddy diffusion coefficient ($\sim 3 \times 10^3$ m^2 yr^{-1}) and the surface area of the oceans (3.6×10^{14} m^2). The condition of steady state further constrains the fluxes in the model. Thus, burial of Se in sediments must balance the external riverine and volcanic inputs. Assuming that the same sedimentation rate applies to the three sedimentary forms of Se, we then obtain the individual burial fluxes from the relative abundances of Se(0), POSe and FeSe (Table 2).

The steady state reservoir sizes and fluxes yield a residence time of 11,500 yrs for reactive Se in the modern ocean. This is within the range of previous estimates from 2300 yrs (Mackenzie et al., 1979) to 26,000 yrs (Broecker and Peng, 1982; Large et al., 2015). They also represent the initial conditions for the numerical simulations and are used to calculate the rate constants (k) for the flux equations. With the exception of the vertical diffusive fluxes between surface and deep-water masses, the model assumes linear flux expressions, that is, the total mass flux of Se from a source reservoir to a receptor reservoir is proportional to the Se mass in the source reservoir (Flux-Mass $* k$). The next section explains how isotopic fractionations are included in the model.

3.2. Marine Se cycle: isotopes

Relatively few data exist to constrain the isotopic compositions of the external Se inputs to the oceans. The $\delta^{82/76}$Se value imposed to the riverine input of DISe (1.05‰) is based on measurements from the San Joaquin River and Sacramento River in California and the Uncompahgre River (Clark and Johnson, 2010; Herbel et al., 2002; Johnson et al., 2000). Volcanic Se(0) inputs are assigned a mantle-like $\delta^{82/76}$Se value of 0‰ (Rouxel et al., 2002; Stüeken et al., 2015b). The riverine Se(0) flux is very small; it is arbitrarily assigned a $\delta^{82/76}$Se value of 0‰. Riverine POSe is assumed to have a $\delta^{82/76}$Se value close to that reported for marine plankton (Mitchell et al., 2012). The isotopic compositions assigned to the sedimentary Se pools yield a bulk shale $\delta^{82/76}$Se value within the range observed for Phanerozoic marine

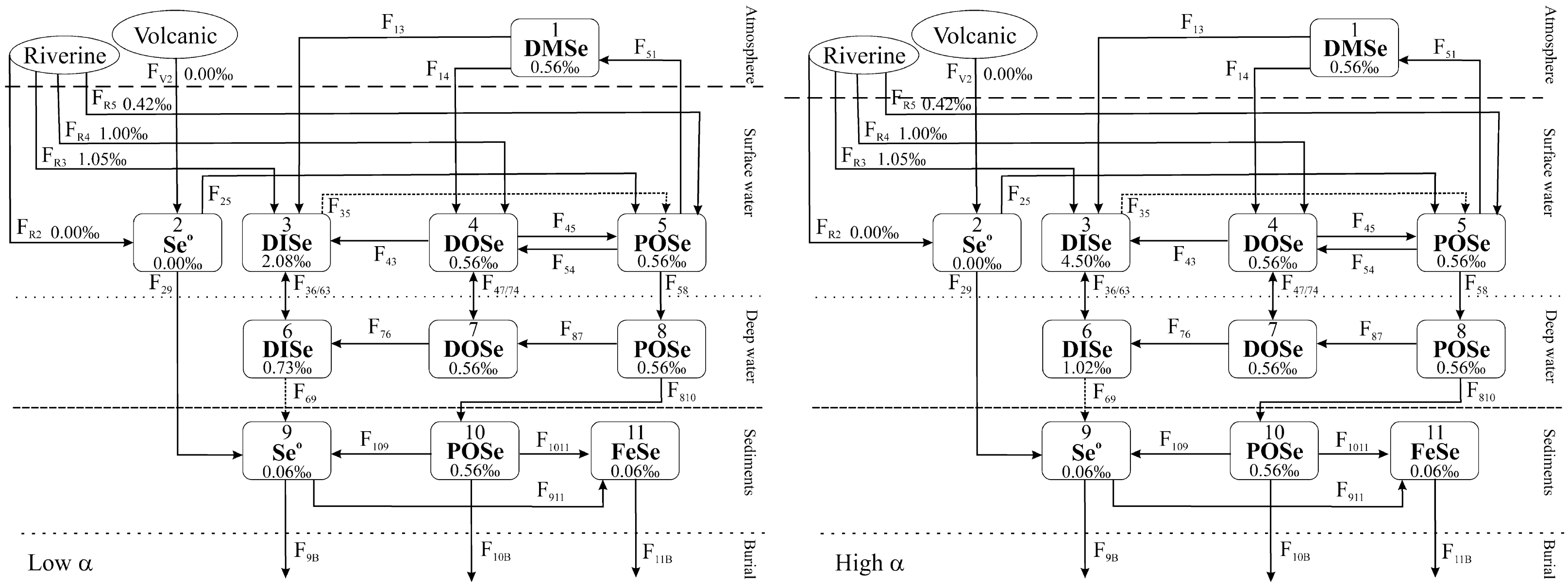

Fig. 3. Modern, pre-anthropogenic biogeochemical cycle of selenium in the oceans. The $\delta^{82/76}$Se values of the various reservoirs are obtained by (1) imposing low and high α values (see text for details) for the assimilatory flux in the surface ocean (F_{35}) and the dissimilatory flux of deep water DISe (F_{69}), and then (2) spinning the model up to steady state. The model assumes that only fluxes F_{35} and F_{69} (dashed lines) are accompanied by isotopic fractionations. R = riverine; V = volcanic; B = burial.

Table 1
Initial steady state reservoir sizes of reactive Se in modern atmosphere, oceans and marine sediments.

	Reservoir	Mass (mol)	Calculation	References
1	Atmosphere, DMSe	1.39×10^7	Directly from reference	(Nriagu, 1989a)
Surface ocean, total		1.33×10^{10}		(Nriagu, 1989a)
2	Surface ocean, DISe	6.49×10^9	61% of total dissolved Se surface ocean	(Cutter and Bruland, 1984)
3	Surface ocean, DOSe	4.15×10^9	39% of total dissolved Se surface ocean	(Cutter and Bruland, 1984)
4	Surface ocean, POSe	2.66×10^9	Chapter 13; Table 1	(Nriagu, 1989a)
5	Surface ocean, Se(0)	2.00×10^6	Extrapolated from known [Se(0)] in rivers and estuaries	(Doblin et al., 2006; Takayanagi and Wong, 1983)
Deep ocean, total		1.96×10^{12}		(Nriagu, 1989a)
6	Deep ocean, DISe	1.53×10^{12}	93% of total dissolved Se deep ocean	(Cutter and Bruland, 1984)
7	Deep ocean, DOSe	1.15×10^{11}	7% of total dissolved Se deep ocean	(Cutter and Bruland, 1984)
8	Deep ocean, POSe	3.17×10^{11}	% particulate matter × [Se] particulate matter × volume	(Buat-Menard and Chesselet, 1979; Mackenzie et al., 1979)
Sediments, total		1.61×10^{11}	~0.42 ppm Se (range 0.1–1.7 ppm Se)	(Mitchell et al., 2012; Sokolova and Pilipchuck, 1973)
9	Sediments, Se(0)	1.43×10^{10}	10%—mean of relative abundances in sediments and rocks	(Wen et al., 2006; Wen and Qiu, 1999)
10	Sediments, POSe	1.00×10^{11}	67%—mean of relative abundances in sediments and rocks	(Cutter, 1985; Kulp and Pratt, 2004)
11	Sediments, FeSe	3.50×10^{10}	23%—mean of relative abundances in sediments and rocks	(Fan et al., 2011; Velinsky and Cutter, 1990)

Table 2
Initial steady state fluxes of reactive Se. R = riverine; V = volcanic; B = burial.

Flux	(mol/yr)	Calculation	References
F_{R2} (Se^0)	5.62×10^7	37% of total particulate Se of riverine flux in Nriagu model	(Doblin et al., 2006; Nriagu, 1989a)
F_{R3} (DISe)	2.37×10^7	89% of total dissolved Se of riverine flux in Nriagu model	(Cutter and Cutter, 2004; Nriagu, 1989a)
F_{R4} (DOSe)	2.93×10^6	11% of total dissolved Se of riverine flux in Nriagu model	(Cutter and Cutter, 2004; Nriagu, 1989a)
F_{R5} (POSe)	9.58×10^7	63% of total particulate Se of riverine flux in Nriagu model	(Doblin et al., 2006; Nriagu, 1989a)
F_{V2} (Se^0)	2.15×10^5	Estimated from values for marine settings in references	(Mosher and Duce, 1989; Nriagu, 1989a; Wen and Carignan, 2007)
F_{13}	1.05×10^8	95% oxidation of volatile DMSe in atmosphere	(Nriagu, 1989a)
F_{14}	2.45×10^8	F_{51}–F_{13}	(Nriagu, 1989a)
F_{51}	3.50×10^8	Directly from reference	(Amouroux et al., 2001)
F_{25}	2.00×10^3	Based on relative uptake rates of Se by phytoplankton	(Harrison et al., 1988; Hu et al., 1997)
F_{35}	4.67×10^8	77% of total Se uptake by plankton (range 47–96%)	(Baines et al., 2001)
F_{43}	1.68×10^8	Based on reported rates of oxidation of organic Se	(Cutter, 1982; Cutter and Bruland, 1984)
F_{45}	1.30×10^9	23% of total Se uptake by plankton (range 4–53%)	(Lee and Fisher, 1993)
F_{54}	1.22×10^9	33% total yearly $POSe_{surface}$ production released as DOSe	(Lee and Fisher, 1993)
F_{29}	5.64×10^7	Based on particle flux from surface to deep ocean	(Buat-Menard and Chesselet, 1979)
$F_{36/63}$	1.71×10^8	Based on average turbulent diffusion coefficient	(Krom et al., 1992)
$F_{47/74}$	1.52×10^6	Based on average turbulent diffusion coefficient	(Krom et al., 1992)
F_{58}	2.95×10^8	13.5 ng cm^{-2} yr^{-1} (Buat-Menard; Table 5) × ocean surface area	(Buat-Menard and Chesselet, 1979, Mackenzie et al., 1979)
F_{69}	5.00×10^4	Based on reduction rates of Se oxyanions in sediments	(Ellis et al., 2003; Oremland et al., 1999; Oremland et al., 1990)
F_{76}	1.71×10^8	Assumes 100% re-oxidation of $DOSe_{deep}$ to $DISe_{deep}$	(Cutter and Bruland, 1984)
F_{87}	1.72×10^8	Assumes ~80% dissolution of F_{58} plus steady state condition	
F_{810}	1.22×10^8	20 μmol C_{org} cm^{-2} yr^{-1} × ocean surface area × (Se:C_{org})	(Emerson et al., 1985; Sherrard et al., 2004)
F_{109}	6.50×10^6	Steady state condition + evidence for organic Se oxidation	(Velinsky and Cutter, 1991)
F_{1110}	1.99×10^3	Early diagenetic Se redistribution based on references	(Wen et al., 2006; Wen and Qiu, 1999; Zhu et al., 2004)
F_{911}	4.36×10^7	Early diagenetic Se redistribution based on references	(Wen et al., 2006; Wen and Qiu, 1999; Zhu et al., 2004)
F_{9B}	1.94×10^7	Total Se burial x fraction total sediment Se as S^0	[Note: at steady state: total ocean Se input = total Se burial]
F_{10B}	1.16×10^8	Total Se burial x fraction total sediment Se as POSe	
F_{11B}	4.36×10^7	Total Se burial x fraction total sediment Se as FeSe	

shales (Mitchell et al., 2012). Isotopic mass balance then requires a $\delta^{82/76}$Se value of 1‰ for the river supply of DOSe.

The largest Se isotope fractionations are associated with reductive processes. The model therefore accounts for the fractionations ($\varepsilon^{82/76}$) associated with assimilatory and dissimilatory Se reduction.

The fractionation factor (α) is defined by the following equation:

$$\alpha_{\text{Product}-\text{Reactant}} = \frac{\left(\frac{^{82}\text{Se}}{^{76}\text{Se}}\right)_{\text{Product}}}{\left(\frac{^{82}\text{Se}}{^{76}\text{Se}}\right)_{\text{Reactant}}} \tag{1}$$

Mass-dependent fractionation during assimilatory (F_{35}—refers to flux numbering system shown in Table 2 and Fig. 3) and dissimilatory (F_{69}) reduction is included in the numerical calculations by adjusting the rate constants of the six individual stable isotopes using the mass bias factor (β), defined as (Albarede and Beard, 2004; Clark and Johnson, 2008):

$$\beta = \frac{\ln\left(\frac{\delta^{82/76}\text{Se}}{1000} + 1\right)}{\ln\left(\frac{A_{82}}{A_{76}}\right)} \tag{2}$$

where A is atomic mass. The mass ratio of the i-th isotope relative to ^{76}Se is then given by

$$r_i = R_i \left(\frac{A_i}{A_{76}}\right)^{\beta} \tag{3}$$

where r_i is the isotope ratio of the sample, and R_i is that of the standard. The fractionation factor (α) of the i-th isotope relative to ^{76}Se is derived from $\alpha^{82/76}$, which in turn is calculated from the imposed isotope fractionation $\varepsilon^{82/76}$ using the relationship ($\varepsilon = \alpha - 1) * 1000$‰ (Canfield, 2001; Mitchell et al., 2012). The rate constant k_{76}, for the ^{76}Se isotope, is related to the total Se mass flux by,

$$k_{76} = \frac{(k_T M_T)}{[\alpha_{74}M_{74} + \alpha_{76}M_{76} + \alpha_{77}M_{77} + \alpha_{78}M_{78} + \alpha_{80}M_{80} + \alpha_{82}M_{82}]} \tag{4}$$

where k_T is the rate constant for the total flux and M_T is the total mass of Se in the source reservoir. The k_{76} value is used along with the α values of the individual isotopes to calculate the isotope-

Table 3
Perturbations imposed on the modern marine Se cycle. For each perturbation two model runs were performed, one with the highest and one with the lowest fractionations for assimilatory and dissimilatory reduction (see main text for further discussion).

Perturbation	Flux modifications
1 Reduced assimilatory uptake	$DISe_{surf} \rightarrow POSe_{surf}$: rate constant decreased by 2 orders of magnitude
2 Anoxic bottom waters	$DOSe_{deep} \rightarrow DISe_{deep} = 0$
	$POSe_{seds} \rightarrow Se(0)_{seds} = 0$
3 Increased dissimilatory reduction	$DISe_{deep} \rightarrow Se(0)_{seds}$: rate constant increased by 2 orders of magnitude
4 P1 + P2 + P3	$DISe_{surf} \rightarrow POSe_{surf}$: rate constant decreased by 2 orders of magnitude
	$DOSe_{deep} \rightarrow DISe_{deep} = 0$
	$POSe_{seds} \rightarrow Se(0)_{seds} = 0$
	$DISe_{deep} \rightarrow Se(0)_{seds}$: rate constant increased by 2 orders of magnitude
5 Anoxic bottom water and increased dissimilatory reduction (P2 + P3)	$DOSe_{deep} \rightarrow DISe_{deep} = 0$
	$POSe_{seds} \rightarrow Se(0)_{seds} = 0$
	$DISe_{deep} \rightarrow Se(0)_{seds}$: rate constant increased by 2 orders of magnitude

specific k values. For example, the first order rate constant for ^{74}Se is given by

$$k_{74} = \alpha_{74} k_{76} \tag{5}$$

The model is initialized by assigning the same average isotopic abundances to all the reservoirs (i.e., all reservoirs have the same initial $\delta^{82/76}$Se value). Next, the model is spun up and the isotopes are redistributed according to the parameters chosen for each case. The fractionations (ε) used for assimilatory and dissimilatory reduction were based on Johnson and Bullen (2004). Assimilatory reduction was assigned a low value of −1.5% and a high value of −3.9‰ and dissimilatory reduction was assigned a low value of −1.7% and a high value of −13.7‰. High and low fractionation cases (both fractionations high, or both low) were considered, to establish a range of possible outcomes. Except for the reductive processes, the isotopes are transferred in the same proportions as they occur in the source reservoir. The model spin-up to steady state yields the baseline $\delta^{82/76}$Se values for the modern ocean shown in Fig. 3.

Importantly, the basic configuration of the model leads to limited variability in the $\delta^{82/76}$Se value of the bulk shale. Unlike S, which can be removed from the ocean as sulfate in evaporite deposits, Se does not have significant burial fluxes of soluble, oxidized species. Accordingly, the only significant output of Se is burial of reduced species in shales. Because the model assumes a steady state and has a single, homogeneous bulk shale output, that output must be isotopically identical to the Se input. This is a trivial result that merely reflects the general characteristics of the Se cycle. The more important results of this model are the quantitative predictions of $\delta^{82/76}$Se values of individual Se species, and of shales with varying proportions of the various Se species.

The model results given in Fig. 3 are a highly simplified version of reality, but provide insights that can be applied to the real world. In the real oceans, the proportions of sedimentary POSe (organically bound Se) and reduced inorganic Se (FeSe and Se(0)) vary from place to place. Areas with high proportions of POSe will have relatively high sedimentary $\delta^{82/76}$Se values, whereas areas with greater proportions of authigenic Se(0) and/or FeSe will have lighter values. Stüeken et al. (2015b) invoked this mechanism as a driver of the difference in mean $\delta^{82/76}$Se between Proterozoic and Phanerozoic sediments: with increased deep-ocean oxygenation, large areas of the ocean floor would begin to collect isotopically light authigenic Se, while remaining anoxic basins would collect the complementary heavy flux. Importantly, our model results (Fig. 3) suggest that the isotopic differences between Se pools are considerably muted relative to the isotopic fractionations occurring during reduction. This is one reason for the small amplitude of bulk shale $\delta^{82/76}$Se variation observed to date.

In an extreme case, local conditions could lead to more strongly negative $\delta^{82/76}$Se values, as observed by Wen et al. (2014) for part of the early Cambrian Yangtze platform. Wen et al. (2014) argued that ferruginous waters provided a strong reducing sink for dissolved, oxidized Se and deposited abundant FeSe and/or Se(0) with low $\delta^{82/76}$Se values to produce bulk shales with $\delta^{82/76}$Se values as low as −5.1‰. We assert that the area of ferruginous waters must have been a local occurrence; global occurrence would have driven the deep ocean water to high $\delta^{82/76}$Se values via a reservoir effect (see below). But a limited area of ferruginous waters could reduce dissolved, oxidized Se drawn from a dominantly oxic ocean with a near-zero $\delta^{82/76}$Se values.

3.3. Perturbations

The perturbations imposed on the model are designed to assess the sensitivity of marine Se isotope systematics to large departures from baseline Se cycling in the modern ocean. Using the same model across geological time assumes that assimilatory uptake of Se was an important biochemical pathway throughout, and that Se was incorporated into the biochemistry of cells during the emergence and evolution of life, possibly even before S (Hengeveld, 2007; Hengeveld and Fedonkin, 2007; Rao et al., 2003; Romero et al., 2005; Sun and Caetano-Anollés, 2009). Because the modern Se cycle is dominated by assimilatory reduction and oxidative recycling of DISe, we focus on perturbations where (1) assimilatory DISe uptake in the surface waters is decreased (Perturbation 1), (2) oxidative recycling in the water column and sediments is inhibited (Perturbation 2), (3) dissimilatory Se reduction is increased (Perturbation 3), and (4) the previous perturbations are combined (Perturbation 4 = Perturbations 1 + 2 + 3, Perturbation 5 = Perturbations 1 + 2). Perturbation 1 is implemented by reducing the rate constant for assimilatory DISe uptake by two orders of magnitude relative to the baseline simulation; in Perturbation 3 the rate coefficient for dissimilatory Se reduction is increased by two orders of magnitude. The 5 perturbations are summarized in Table 3. Additional perturbations were tested in which we varied the intensity of exchanges between the surface and deep-water masses (results not shown). These all yielded isotopic shifts that fall within the ranges obtained with the 5 perturbations described above.

Because of the short oceanic residence time of reactive Se, the model rapidly converges to a new steady state after imposing a given perturbation. In addition, because the Se inputs to the ocean are kept constant, the new bulk steady state sediment $\delta^{82/76}$Se values are identical to those in the baseline simulation (see explanation above). Thus, our analysis focuses on the effects of the perturbations on the $\delta^{82/76}$Se values of individual water column and sediment Se reservoirs. For each perturbation, two sets of simulations are carried out, one with the highest $\varepsilon^{82/76}$ values for assimilatory (−3.9‰) and dissimilatory reduction (−13.7‰) reported by Johnson and Bullen (2004), the other with their lowest values (−1.5‰ and −1.7‰, respectively). The resulting changes in

Table 4
Initial $\delta^{82/76}$Se values for the marine Se cycle and changes in $\delta^{82/76}$Se ($\Delta\delta^{82/76}$Se) for the high and low α cases in each of the perturbation scenarios. The changes are expressed relative to the initial $\delta^{82/76}$Se values.

Reservoirs	Initial		Scenario 1		Scenario 2		Scenario 3		Scenario 4		Scenario 5	
	High α	Low α	High	Low	High	Low	High	Low	High	Low	High	Low
	$\delta^{82/76}$Se (‰)		$\Delta\delta^{82/76}$Se (‰)									
DMSe (atm)	0.557	0.556	0.010	0.000	−0.001	0.000	0.124	0.014	0.669	0.010	0.006	0.000
Se(0) (surf)	0.000	0.000	0.000	0.000	0.000	0.000	0.000	0.000	0.000	0.000	0.000	0.000
DISe (surf)	4.495	2.083	0.012	0.000	0.010	0.011	0.152	0.018	0.917	0.029	0.020	0.011
DOSe (surf)	0.558	0.557	0.010	0.000	−0.001	0.000	0.124	0.014	0.668	0.010	0.006	0.000
POSe (surf)	0.557	0.556	0.010	0.000	−0.001	0.000	0.124	0.014	0.669	0.010	0.006	0.000
DISe (deep)	1.016	0.734	3.214	1.241	3.490	1.360	0.217	0.025	4.489	1.389	3.591	1.372
DOSe (deep)	0.557	0.556	0.010	0.000	−0.001	0.000	0.124	0.014	0.669	0.010	0.006	0.000
POSe (deep)	0.557	0.556	0.010	0.000	−0.001	0.000	0.124	0.014	0.669	0.010	0.006	0.000
Se(0) (seds)	0.055	0.057	−0.019	0.001	−0.055	−0.057	−0.213	−0.017	−1.152	−0.001	−0.071	−0.057
POSe (seds)	0.557	0.556	0.010	0.000	−0.001	0.000	0.124	0.014	0.669	0.010	0.006	0.000
FeSe (seds)	0.055	0.057	−0.019	0.001	−0.055	−0.057	−0.213	−0.017	−1.152	−0.001	−0.071	−0.057

$\delta^{82/76}$Se of the various Se reservoirs are summarized in Table 4 for all five scenarios.

As expected, the largest isotopic shifts are observed when imposing the highest fractionations to assimilatory and dissimilatory reduction. Furthermore, the $\delta^{82/76}$Se of the deep water DISe reservoir is most sensitive to the perturbations. A decrease in assimilatory Se uptake (Perturbation 1), the inhibition of oxidative recycling (Perturbation 2) and combinations of both (Perturbations 4 and 5) produce heavier deep water DISe. In these cases, surface water DISe concentration exceeds that of the deep water, hence causing downward diffusive transport of DISe in the water column. The remaining sink for deep water DISe is dissimilatory reduction, which removes lighter isotope preferentially and leaves behind isotopically heavier DISe with $\delta^{82/76}$Se up to 4.5‰ higher than in the baseline case. Perturbation 3 does not cause a reversal in the concentration gradient of DISe between surface and deep waters and, consequently, the corresponding increase in the $\delta^{82/76}$Se of deep water DISe is markedly smaller (<1‰).

No data currently exist on the Se isotopic composition of past, or even present, seawater. The modeling results suggest, however, that the isotopic composition of seawater DISe could be a sensitive indicator of marine paleoredox conditions and the oceanic Se recycling efficiency. Hence, reconstructing past seawater $\delta^{82/76}$Se by, for example, extracting Se from evaporite or carbonate minerals, could yield valuable proxy information, similar to that derived from the seawater sulfate isotopic record (e.g., Paytan et al., 1998).

The model indicates that the sedimentary Se reservoirs are also sensitive to the imposed perturbations, but to a lesser extent. The largest changes are observed for Perturbation 4, with a maximum drop in $\delta^{82/76}$Se of 1.2‰ for sedimentary Se(0) and FeSe, and a maximum increase of 0.7‰ for organic Se. For the other perturbations, changes in $\delta^{82/76}$Se for all the sedimentary pools are below 1‰ and do not approach the +3 and −3‰ variability seen in the shale data. This can only be achieved by setting the model input values to unrealistically high values in excess of 25‰. The small amplitude of the sedimentary Se(0) and FeSe response is caused by a reservoir effect: Strong dissimilatory reduction and/or large dissimilatory fractionation drives deep water DISe to heavier values, offsetting part of the fractionation. The even smaller organic Se response stems from its sourcing from surface waters, which have a relatively muted response to deep water DISe reduction. Thus, even when conditions favor a marine Se cycle dominated by dissimilatory reduction and limited oxidative recycling of DOSe, for example during an ocean anoxic event, the responses of the sedimentary components are much smaller than the isotopic fractionations driving them. However, with $\delta^{82/76}$Se analytical precision approaching ±0.1‰ and the potential for extracting the various Se pools selectively (Cutter, 1985; Kulp and Pratt, 2004; Velinsky and Cutter, 1990), it is likely that measurement of individual Se pools will provide a sensitive paleoredox proxy.

4. Conclusions

Bulk $\delta^{82/76}$Se values measured on marine shales from 3.25 Ga to the present day fall within a limited range between −3 and +3‰. No global systematic $\delta^{82/76}$Se shifts are observed across the Great Oxidation Event, but a minor shift to more negative values is observed from Precambrian to Phanerozoic samples. Muted isotopic fractionation in the marine system is most likely due to the dominance of assimilatory uptake of Se into biomass that began at least at 3.25 Ga, together with the persistence of low seawater Se concentrations and a roughly uniform isotopic composition of reactive Se delivered to the oceans through time.

Isotope mass balance calculations confirm that bulk shale $\delta^{82/76}$Se values are insensitive to even large changes in water column redox conditions, primary productivity and ocean circulation. The relatively short marine residence time of roughly 11,500 yrs for Se in the modern ocean, combined with the lack of a large alternative Se sink with contrasting Se isotopic composition (i.e. evaporites), implies that bulk marine shale $\delta^{82/76}$Se values primarily reflect the collective isotopic composition of the reactive Se inputs to the oceans. Some spatial variation in bulk $\delta^{82/76}$Se values should occur as a result of differences in the relative fluxes of organically bound Se and authigenic Se (Stüeken et al., 2015b; Wen et al., 2014), but in most cases these differences tend to be somewhat muted because of the characteristics of the Se cycle.

Our modeling results indicate that changes in the isotopic composition of seawater Se over time, and, equally important, isotopic differences between the various forms of sedimentary Se have the potential to yield valuable information on past ocean biogeochemistry. These should thus be priority research areas supporting the further development of Se isotopic proxies for paleoceanographic applications. Although the models indicate the $\delta^{82/76}$Se contrasts tend to be somewhat muted because of the characteristics of the Se cycle, the $\delta^{82/76}$Se contrasts are likely large enough to provide a sensitive paleoredox proxy.

Acknowledgements

This work was supported by a grant number 864.04.008 from the Netherlands Organization for Scientific Research (NWO).

Appendix A. Supplementary material

Supplementary material related to this article can be found online at http://dx.doi.org/10.1016/j.epsl.2016.02.030.

References

Albarede, F., Beard, B., 2004. Analytical methods for non-traditional isotopes. Rev. Mineral. Geochem. 55, 113–152.

Amouroux, D., Liss, P.S., Tessier, E., Hamren-Larsson, M., Donard, O.F.X., 2001. Role of oceans as biogenic sources of selenium. Earth Planet. Sci. Lett. 189, 277–283.

Baines, S.B., Fisher, N.S., Doblin, M.A., Cutter, Gregory A., 2001. Uptake of dissolved organic selenides by marine phytoplankton. Limnol. Oceanogr. 46, 1936–1944.

Berner, R.A., Canfield, D.E., 1989. A new model for atmospheric oxygen over Phanerozoic time. Am. J. Sci. 289, 333–361.

Böttcher, M.E., Thamdrup, B., 2001. Oxygen and sulfur isotope fractionation during anaerobic bacterial disproportionation of elemental sulfur. Geochim. Cosmochim. Acta 65, 1601–1609.

Bontognali, T.R.R., Sessions, A.L., Allwood, A.C., Fischer, W.W., Grotzinger, J.P., Summons, R.E., Eiler, J.M., 2012. Sulfur isotopes of organic matter preserved in 3.45-billion-year-old stromatolites reveal microbial metabolism. Proc. Natl. Acad. Sci. 109, 15146–15151.

Brocks, J.J., Summons, R.E., Holland, H.D., Karl, K.T., 2003. Sedimentary hydrocarbons, biomarkers for early life. In: Treatise on Geochemistry, vol. 8. Pergamon, Oxford, pp. 63–115.

Broecker, W.S., Peng, T.H., 1982. Tracers in the Sea. Eldigio Press Lamont Doherty Geological Observatory.

Buat-Menard, P., Chesselet, R., 1979. Variable influence of the atmospheric flux on the trace metal chemistry of oceanic suspended matter. Earth Planet. Sci. Lett. 42, 399–411.

Canfield, D.E., 2001. Biogeochemistry of sulfur isotopes. Rev. Mineral. Geochem. 43, 607–636.

Canfield, D.E., 2004. The evolution of the Earth surface sulfur reservoir. Am. J. Sci. 304, 839–861.

Canfield, D.E., 2005. The early history of atmospheric oxygen: homage to Robert A. Garrels. Annu. Rev. Earth Planet. Sci. 33, 1–36.

Canfield, D.E., Farquhar, J., 2009. Animal evolution, bioturbation, and the sulfate concentration of the oceans. Proc. Natl. Acad. Sci. 106, 8123–8127.

Canfield, D.E., Habicht, K.S., Thamdrup, B., 2000. The Archean sulfur cycle and the early history of atmospheric oxygen. Science 288, 658–661.

Canfield, D.E., Kristensen, E., Thamdrup, B., 2005. The sulfur cycle. In: Advances in Marine Biology, vol. 48. Academic Press, pp. 313–381.

Canfield, D.E., Poulton, S.W., Narbonne, G.M., 2007. Late-neoproterozoic deep-ocean oxygenation and the rise of animal life. Science 315, 92–95.

Canfield, D.E., Raiswell, R., 1999. The evolution of the sulfur cycle. Am. J. Sci. 299, 697–723.

Canfield, D.E., Teske, A., 1996. Late Proterozoic rise in atmospheric oxygen concentration inferred from phylogenetic and sulphur-isotope studies. Nature 382, 127–132.

Chambers, L., 1975. Fractionation of sulfur isotopes by continuous cultures of Desulfovibrio desulfuricans. Can. J. Microbiol. 21, 1602–1607.

Clark, S.K., Johnson, T.M., 2008. Effective isotopic fractionation factors for solute removal by reactive sediments: a laboratory microcosm and slurry study. Environ. Sci. Technol. 42, 7850–7855.

Clark, S.K., Johnson, T.M., 2010. Selenium stable isotope investigation into selenium biogeochemical cycling in a lacustrine environment: Sweitzer Lake, Colorado. J. Environ. Qual. 39, 2200–2210.

Copeland, P., 2005. Making sense of nonsense: the evolution of selenocysteine usage in proteins. Genome Biol. 6, 221.

Cutter, G.A., 1982. Selenium in reducing waters. Science 217, 829–831.

Cutter, G.A., 1985. Determination of selenium speciation in biogenic particles and sediments. Anal. Chem. 57, 2951–2955.

Cutter, G.A., Bruland, K.W., 1984. The marine biogeochemistry of selenium: a re-evaluation. Limnol. Oceanogr. 29, 1179–1192.

Cutter, G.A., Cutter, L.S., 1995. Behavior of dissolved antimony, arsenic, and selenium in the Atlantic Ocean. Mar. Chem. 49, 295–306.

Cutter, G.A., Cutter, L.S., 2004. Selenium biogeochemistry in the San Francisco Bay estuary: changes in water column behavior. Estuar. Coast. Shelf Sci. 61, 463–476.

Doblin, M.A., Baines, S.B., Cutter, L.S., Cutter, G.A., 2006. Sources and biogeochemical cycling of particulate selenium in the San Francisco Bay estuary. Estuar. Coast. Shelf Sci. 67, 681–694.

Eigen, M., Lindemann, B., Tietze, M., Winkler-Oswatitsch, R., Dress, A., von Haeseler, A., 1989. How old is the genetic code? Statistical geometry of tRNA provides an answer. Science 244, 673–679.

Ellis, A.S., Johnson, T.M., Bullen, T.D., 2002. Chromium isotopes and the fate of hexavalent chromium in the environment. Science 295, 2060–2062.

Ellis, A.S., Johnson, T.M., Herbel, M.J., Bullen, T.D., 2003. Stable isotope fractionation of selenium by natural microbial consortia. Chem. Geol. 195, 119–129.

Emerson, S., Fischer, K., Reimers, C., Heggie, D., 1985. Organic carbon dynamics and preservation in deep-sea sediments. Deep-Sea Res., A, Oceanogr. Res. Pap. 32, 1–21.

Fan, H., Wen, H., Hu, R., Zhao, H., 2011. Selenium speciation in Lower Cambrian Se-enriched strata in South China and its geological implications. Geochim. Cosmochim. Acta 75, 7725–7740.

Habicht, K.S., Canfield, D.E., 1997. Sulfur isotope fractionation during bacterial sulfate reduction in organic-rich sediments. Geochim. Cosmochim. Acta 61, 5351–5361.

Harrison, A.G., Thode, H.G., 1958. Mechanism of the Bacterial Reduction of Sulphate from isotope fractionation studies. Trans. Faraday Soc. 53, 84–92.

Harrison, P.J., Yu, P.W., Thompson, P.A., Price, N.M., Phillips, D.J., 1988. Survey of selenium requirements in marine phytoplankton. Mar. Ecol. Prog. Ser. 47, 89–96.

Hengeveld, R., 2007. Two approaches to the study of the origin of life. Acta Biotheor. 55, 97–131.

Hengeveld, R., Fedonkin, M., 2007. Bootstrapping the energy flow in the beginning of life. Acta Biotheor. 55, 181–226.

Herbel, M.J., Johnson, T.M., Oremland, R.S., Bullen, T.D., 2000. Fractionation of selenium isotopes during bacterial respiratory reduction of selenium oxyanions. Geochim. Cosmochim. Acta 64, 3701–3709.

Herbel, M.J., Johnson, T.M., Tanji, K.K., Gao, S.D., Bullen, T.D., 2002. Selenium stable isotope ratios in California agricultural drainage water management systems. J. Environ. Qual. 31, 1146–1156.

Hu, M., Yang, Y., Martin, J.M., Yin, K., Harrison, P.J., 1997. Preferential uptake of Se(IV) over Se(VI) and the production of dissolved organic Se by marine phytoplankton. Mar. Environ. Res. 44, 225–231.

Johnson, T.M., Bullen, T.D., 2003. Selenium isotope fractionation during reduction by Fe(II)–Fe(III) hydroxide-sulfate (green rust). Geochim. Cosmochim. Acta 67, 413–419.

Johnson, T.M., Bullen, T.D., 2004. Mass-dependent fractionation of selenium and chromium isotopes in low-temperature environments. Rev. Mineral. Geochem. 55, 289–317.

Johnson, T.M., Bullen, T.D., Zawislanski, P.T., 2000. Selenium stable isotope ratios as indicators of sources and cycling of selenium: results from the northern reach of San Francisco Bay. Environ. Sci. Technol. 34, 2075–2079.

Kaplan, I.R., Rittenberg, S.C., 1964. Microbiological fractionation of sulphur isotopes. J. Gen. Microbiol. 34, 195–212.

Krom, M.D., Brenner, S., Kress, N., Neori, A., Gordon, L.I., 1992. Nutrient dynamics and new production in a warm-core eddy from the Eastern Mediterranean Sea. Deep-Sea Res., A, Oceanogr. Res. Pap. 39, 467–480.

Krouse, H.R., Thode, H.G., 1962. Thermodynamic properties and geochemistry of isotopic compounds of selenium. Can. J. Chem. 40, 367–375.

Kulp, T.R., Pratt, L.M., 2004. Speciation and weathering of selenium in upper cretaceous chalk and shale from South Dakota and Wyoming, USA. Geochim. Cosmochim. Acta 68, 3687–3701.

Large, R.R., Halpin, J.A., Lounejeva, E., Danyushevsky, L.V., Maslennikov, V.V., Gregory, D., Sack, P.J., Haines, P.W., Long, J.A., Makoundi, C., Stepanov, A.S., 2015. Cycles of nutrient trace elements in the Phanerozoic ocean. Gondwana Res. 28, 1282–1293.

Lee, B.-G., Fisher, N.S., 1993. Release rates of trace elements and protein from decomposing planktonic debris. 1. Phytoplankton debris. J. Mar. Res. 51, 391–421.

Li, X.F., Liu, Y., 2011. Equilibrium Se isotope fractionation parameters: a first-principles study. Earth Planet. Sci. Lett. 304, 113–120.

Mackenzie, F., Lantzy, R., Paterson, V., 1979. Global trace metal cycles and predictions. Math. Geol. 11, 99–142.

Measures, C.I., Burton, J.D., 1980. The vertical distribution and oxidation states of dissolved selenium in the northeast Atlantic Ocean and their relationship to biological processes. Earth Planet. Sci. Lett. 46, 385–396.

Measures, C.I., Grant, B.C., Mangum, B.J., Edmond, J.M., 1983. The relationship of the distribution of dissolved selenium IV and VI in three oceans to the physical and biological process. In: Wong, C.S., Boyle, E., Bruland, K.W., Burton, J.D., Goldberg, E.D. (Eds.), Trace Metals in Sea Water. In: NATO Conference Series IV, Marine Sciences, vol. 9. Plenum Press, New York.

Mitchell, K., Mason, P.R.D., Van Cappellen, P., Johnson, T.M., Gill, B.C., Owens, J.D., Diaz, J., Ingall, E.D., Reichart, G.-J., Lyons, T.W., 2012. Selenium as paleo-oceanographic proxy: a first assessment. Geochim. Cosmochim. Acta 89, 302–317.

Mosher, B.W., Duce, R.A., 1989. The atmosphere. In: Inhat, M. (Ed.), Occurrence and Distribution of Selenium. CRC Press, Boca Raton, pp. 295–325.

Nriagu, J., 1989a. Global cycling of selenium. In: Inhat, M. (Ed.), Occurrence and Distribution of Selenium. CRC Press, Boca Raton, Florida, pp. 327–340.

Nriagu, J., 1989b. Selenium in geological materials. In: Inhat, M. (Ed.), Occurence and Distribution of Selenium. CRC Press, Boca Raton.

Oremland, R.S., Blum, J.S., Bindi, A.B., Dowdle, P.R., Herbel, M.J., Stolz, J.F., 1999. Simultaneous reduction of nitrate and selenate by cell suspensions of selenium-respiring bacteria. Appl. Environ. Microbiol. 65, 4385–4392.

Oremland, R.S., Steinberg, N.A., Maest, A.S., Miller, L.G., Hollibaugh, J.T., 1990. Measurement of in situ rates of selenate removal by dissimilatory bacterial reduction in sediments. Environ. Sci. Technol. 24, 1157–1164.

Paytan, A., Kastner, M., Campbell, D., Thiemens, M.H., 1998. Sulfur isotopic composition of Cenozoic seawater sulfate. Science 282, 1459–1462.

Pogge Von Strandmann, P.A.E., Stüeken, E.E., Elliott, T., Poulton, S.W., Dehler, C.M., Canfield, D.E., Catling, D.C., 2015. Selenium isotope evidence for progressive oxidation of the Neoproterozoic biosphere. Nat. Commun. 6, 10157.

Price, N.M., Thompson, P.A., Harrison, P.J., 1987. Selenium: an essential element for growth of the coastal marine diatom *Thalassiosira Pseudonana* (Bacillariophyceae). J. Phycol. 23, 1–9.

Rao, M., Carlson, B.A., Novoselov, S.V., Weeks, D.P., Gladyshev, V.N., Hatfield, D.L., 2003. Chlamydomonas reinhardtii selenocysteine tRNA[Ser]Sec. RNA 9, 923–930.

Romero, H., Zhang, Y., Gladyshev, V., Salinas, G., 2005. Evolution of selenium utilization traits. Genome Biol. 6, R66.

Rouxel, O., Ludden, J., Carignan, J., Marin, L., Fouquet, Y., 2002. Natural variations of Se isotopic composition determined by hydride generation multiple collector inductively coupled plasma mass spectrometry. Geochim. Cosmochim. Acta 66, 3191–3199.

Sherrard, J.C., Hunter, K.A., Boyd, P.W., 2004. Selenium speciation in subantarctic and subtropical waters east of New Zealand: trends and temporal variations. Deep-Sea Res., Part 1, Oceanogr. Res. Pap. 51, 491–506.

Shore, A., 2010. Selenium geochemistry and isotopic composition of sediments from the Cariaco Basin and the Bermuda Rise: a comparison between a restricted basin and the open ocean over the last 500 ka. University of Leicester.

Sim, M.S., Bosak, T., Ono, S., 2011. Large sulfur isotope fractionation does not require disproportionation. Science 333, 74–77.

Sokolova, Y.G., Pilipchuck, M.F., 1973. Geochemistry of selenium in sediments in the NW part of the Pacific Ocean. Geochem. Int. 10, 1537–1546.

Stüeken, E.E., Buick, R., Anbar, A.D., 2015a. Selenium isotopes support free O_2 in the latest Archean. Geology 43, 259–262.

Stüeken, E.E., Buick, R., Bekker, A., Catling, D., Foriel, J., Guy, B.M., Kah, L.C., Machel, H.G., Montañez, I.P., Poulton, S.W., 2015b. The evolution of the global selenium cycle: secular trends in Se isotopes and abundances. Geochim. Cosmochim. Acta 162, 109–125.

Stüeken, E.E., Foriel, J., Buick, R., Schoepfer, S.D., 2015c. Selenium isotope ratios, redox changes and biological productivity across the end-Permian mass extinction. Chem. Geol. 410, 28–39.

Sun, F.J., Caetano-Anollés, G., 2009. The evolutionary significance of the long variable arm in transfer RNA. Complexity 14, 26–39.

Suzuki, Y., Miyake, Y., Saruhashi, K., Sugimura, Y., 1979. A cycle of selenium in the Ocean. Pap. Meteorol. Geophys. 30, 185–189.

Takayanagi, K., Wong, G.T.F., 1983. Organic and colloidal selenium in Southern Chesapeake Bay and adjacent waters. Mar. Chem. 14, 141–148.

Thode, H.G., Kleerkoper, H., McElcheran, D.E., 1951. Sulfur isotope fractionation in the bacterial reduction of sulfate. Res. London 4, 581–582.

Velinsky, D.J., Cutter, G.A., 1990. Determination of elemental selenium and pyrite-selenium in sediments. Anal. Chim. Acta 235, 419–425.

Velinsky, D.J., Cutter, G.A., 1991. Geochemistry of selenium in a coastal salt marsh. Geochim. Cosmochim. Acta 55, 179–191.

Wen, H., Carignan, J., 2007. Reviews on atmospheric selenium: emissions, speciation and fate. Atmos. Environ. 41, 7151–7165.

Wen, H., Carignan, J., 2011. Selenium isotopes trace the source and redox processes in the black shale-hosted Se-rich deposits in China. Geochim. Cosmochim. Acta 75, 1411–1427.

Wen, H., Carignan, J., Chu, X., Fan, H., Cloquet, C., Huang, J., Zhang, Y., Chang, H., 2014. Selenium isotopes trace anoxic and ferruginous seawater conditions in the Early Cambrian. Chem. Geol. 390, 164–172.

Wen, H., Carignan, J., Hu, R., Fan, H., Chang, B., Yang, G., 2007. Large selenium isotopic variations and its implication in the Yutangba Se deposit, Hubei Province, China. Chin. Sci. Bull. 52, 2443–2447.

Wen, H., Carignan, J., Qiu, Y., Liu, S., 2006. Selenium speciation in kerogen from two Chinese selenium deposits: environmental implications. Environ. Sci. Technol. 40, 1126–1132.

Wen, H., Qiu, Y., 1999. Organic and inorganic occurrence of selenium in Laerma Se–Au deposit. Sci. China, Ser. B, Chem. Life Sci. Earth Sci. 42, 662–669.

Wortmann, U.G., Bernasconi, S.M., Böttcher, M.E., 2001. Hypersulfidic deep biosphere indicates extreme sulfur isotope fractionation during single-step microbial sulfate reduction. Geology 29, 647–650.

Wrench, J.J., 1978. Selenium metabolism in the Marine phytoplankters Tetraselmis tetrathele and Dunaliella minuta. Mar. Biol. 49, 231–236.

Zhu, J.-M., Johnson, T.M., Clark, S.K., Zhu, X.-K., 2008. High precision measurement of selenium isotopic composition by hydride generation Multiple Collector Inductively Coupled Plasma Mass Spectrometry with a ^{74}Se–^{77}Se double spike. Chin. J. Anal. Chem. 36, 1385–1390.

Zhu, J.-M., Johnson, T.M., Clark, S.K., Zhu, X.-K., Wang, X.-L., 2014. Selenium redox cycling during weathering of Se-rich shales: a selenium isotope study. Geochim. Cosmochim. Acta 126, 228–249.

Zhu, J., Zuo, W., Liang, X., Li, S., Zheng, B., 2004. Occurrence of native selenium in Yutangba and its environmental implications. Appl. Geochem. 19, 461–467.